ISLANDED MINIGRID RENEWABLE POWER SYSTEM

Resilient Adaptive VSG Control of a Renewable-Rich Islanded Microgrid: Dynamic Assessment and Resilience Framework

Olusegun Alfred Adeyinka, Abdullahi Abubakar Kehinde, Mariam Omolara Oyelade-Ahmed, Sulaimon Olawale Nurudeen, Tumba Drambi Yohanna

National Space Research and Development Agency (NASRDA), Obasanjo Space Centre, Abuja, Nigeria

Published November 2026

Abstract

A resilient adaptive virtual synchronous generator (VSG) control framework is developed and evaluated for a 50-kW photovoltaic (PV)–battery islanded microgrid exposed to significant load changes and renewable-generation variability. The study employs 15-second dynamic simulations to compare conventional droop control with adaptive VSG control, assessing AC voltage, frequency, rate of change of frequency (RoCoF), battery power, state of charge (SOC), DC-link voltage, efficiency, power factor, current, and a modeled voltage-THD indicator. Results indicate that adaptive VSG reduces the visible peak frequency excursion and RoCoF compared to conventional droop control. However, the current tuning also yields substantially larger AC-voltage excursions and a more pronounced battery discharge response. These findings show that resilience assessment requires considering coordinated frequency, voltage, DC-link, and battery constraints, not frequency performance alone. Accordingly, a multi-objective resilience framework is formulated that adapts virtual inertia, damping, voltage-support gains, and battery support based on renewable/load disturbance severity and battery operating state. This approach establishes a dynamic baseline and a reproducible resilience-assessment framework that can be extended to additional external disturbances in future research.

Keywords: adaptive VSG; battery energy storage; islanded microgrid; photovoltaic generation; resilience; virtual inertia; frequency stability; voltage stability

1 Introduction

Renewable-rich islanded microgrids experience rapid fluctuations in generation and load and have significantly less physical inertia than conventional utility grids. As converter-interfaced PV generation increases, grid-forming inverter controls and battery energy storage systems become essential for maintaining frequency and voltage stability. Substantial renewable fluctuations, load steps, and power imbalances can cause rapid frequency changes, voltage excursions, and higher battery power demands.

Virtual synchronous generator (VSG) control offers a practical method to emulate the inertial and damping characteristics of synchronous machines within converter-dominated microgrids. Fixed VSG parameters, however, often require a compromise between rapid disturbance rejection and acceptable voltage or battery stress. In contrast, adaptive VSG control can adjust its dynamic response based on the severity of instantaneous power imbalances and available energy-storage capacity.

Recent studies demonstrate that adaptive VSG parameters can enhance frequency response under load and PV uncertainty, while hierarchical control structures enable coordination of primary and

secondary functions [1]–[9]. This work focuses on the dynamic resilience of a renewable-rich islanded microgrid, specifically examining the frequency–voltage–battery trade-offs introduced by adaptive virtual inertia and damping.

The supplied simulations provide a useful disturbance benchmark. They contain a 45-kW maximum load, PV variability of approximately 15–49 kW, a critical renewable-generation deficit of approximately 23 kW around 6–7 s, and large positive and negative load steps. The results additionally provide frequency, RoCoF, AC voltage, battery power, SOC, DC-link voltage, efficiency, power factor, current, P–Q response, and a modeled THD indicator.

The primary contributions of this paper are as follows: (1) dynamic interpretation of the supplied conventional-droop and adaptive-VSG results; (2) identification of frequency–voltage–battery trade-offs in current controller tuning; (3) formulation of a disturbance-severity-based adaptive VSG control structure; (4) integration of adaptive voltage support and battery-energy constraints into the resilience framework; and (5) definition of reproducible resilience-performance indices for future validation.

2 50-kW islanded microgrid and baseline disturbances

The microgrid is a 50-kW, 400-V, 50-Hz three-phase islanded system with a 100-kWh battery, 700-V DC-link reference, and 40-kW battery power limit. The model is averaged and control-oriented rather than a semiconductor-switching model. Table 1 summarizes its principal parameters, and Figure 1 shows the Simulink implementation of the controller model.

Table 1. Microgrid system parameters.

Parameter	Value
Rated inverter power	50 kW
AC voltage	400 V line-line RMS
Frequency	50 Hz
PV rating	50 kW
Battery energy	100 kWh
Initial SOC	80%
SOC operating range	20–95%
DC-link reference	700 V
Battery limit	40 kW
Charge/discharge efficiency	95%
Simulation time	15 s
Sample time	100 μs

The baseline load sequence is approximately 0, 10, 20, 45, 15, 45, and 5 kW. PV irradiance changes from approximately 850 to 1000, 650, 950, 450, 800, 300, 900, 500, 750, and 950 W/m^2, producing substantial renewable variability. The maximum 45-kW load corresponds to approximately 90% of the inverter rating. The load, PV and power-balance profiles used for the assessment are shown in Figure 2.

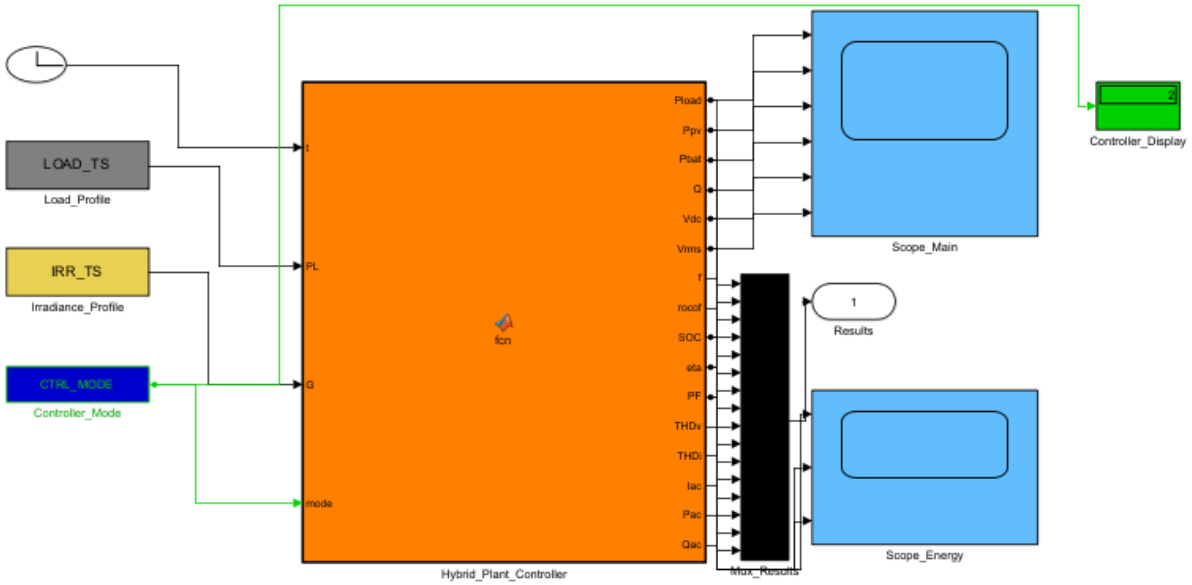


Figure 1. Simulink implementation block diagram of the hybrid PV–battery microgrid controller model.

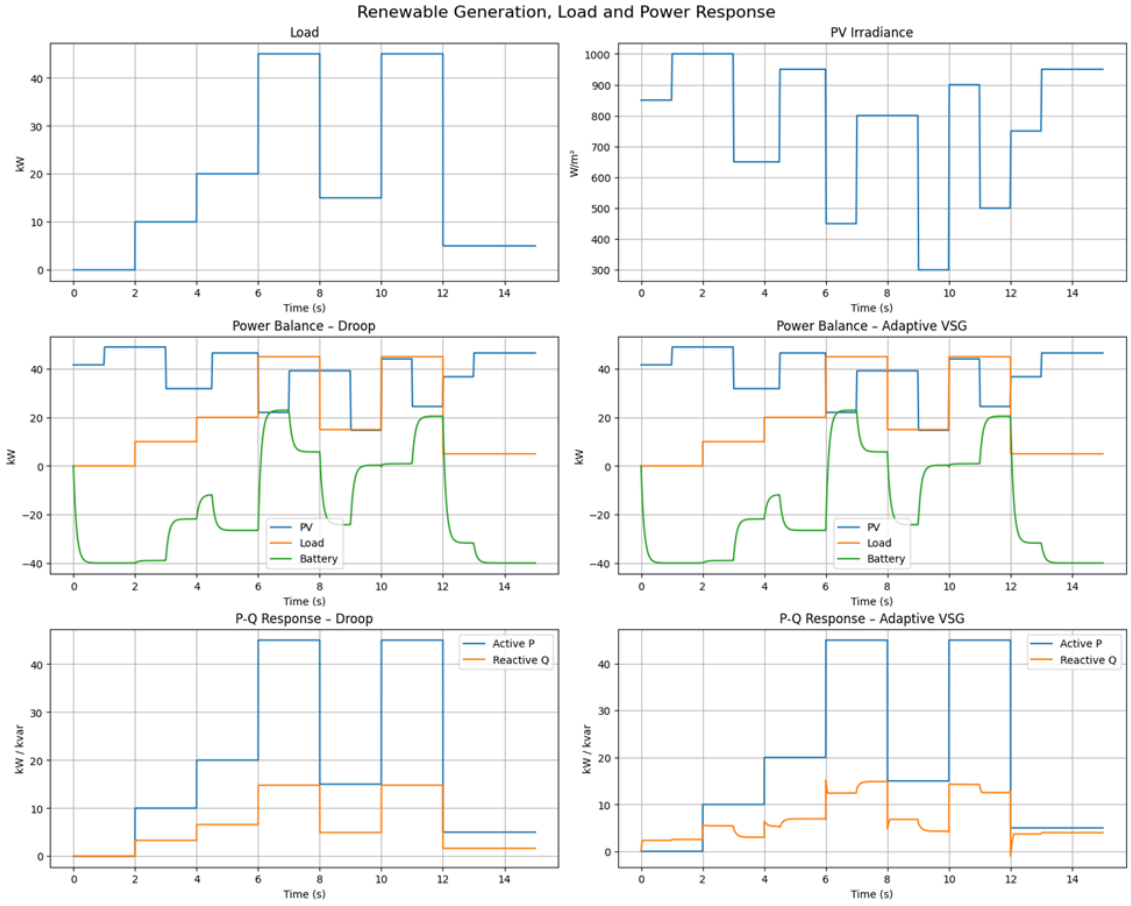


Figure 2. Baseline renewable generation, load, and power response used for the controller assessment.

3 Resilient adaptive VSG control

3.1 Adaptive virtual inertia and damping

The VSG frequency dynamics are represented by

$$2H\left(t\right)\frac{d\omega}{dt} = P^{*} - P_{e} - D\left(t\right)\left(\omega - \omega_{0}\right) \quad (1)$$

The adaptive controller represents operating disturbance severity using the normalized active-power imbalance and battery state. A general disturbance index is defined as

$$S = \alpha S_{PV/L} + \gamma S_{SOC} \quad (2)$$

$$H(t) = H_{0} + K_{H}S,\ D(t) = D_{0} + K_{D}S \quad (3)$$

The first term represents load/PV disturbance severity, and the second represents battery-energy availability. The SOC term is essential because the controller should not demand excessive synthetic inertia from a battery approaching its energy limits. The adaptive gains are bounded to preserve converter operating limits.

3.2 Adaptive voltage control

The supplied baseline results reveal a critical issue: the adaptive VSG frequency response is visually tighter than the droop response, but its AC voltage excursion is much larger. This indicates that frequency adaptation alone is insufficient. A coordinated voltage law is therefore required:

$$Q^{*} = Q_{0} + K_{Q,V}\left(S\right)\left(V_{0} - V\right) + K_{Q,d}\frac{dV}{dt} \quad (4)$$

The voltage-control gains only increase when required and remain bounded by the inverter's reactive-power capability. This prevents frequency-stability improvement at the expense of unacceptable voltage excursions.

3.3 Battery energy management

Battery power should be decomposed into fast support and energy-management components:

$$P_{B}^{*} = P_{VSG} + P_{sec} + P_{EMS} \quad (5)$$

During severe load or renewable disturbances, the reserve SOC is preserved so the battery remains available for subsequent events.

4 Baseline simulation results

Figure 3 compares the two controllers under the baseline disturbance sequence, and the approximate values read from the plots are summarized in Table 2.



Figure 3. Controller comparison for the 50-kW hybrid PV–battery microgrid: AC RMS voltage, frequency, RoCoF, battery power, SOC, DC-link voltage, modeled inverter efficiency, and power factor.

The frequency response remains close to the 50-Hz reference for both controllers. From the plotted traces, the conventional droop case reaches a maximum visible excursion of approximately +0.0048 Hz and −0.0048 Hz, whereas the adaptive VSG remains within approximately +0.003 Hz and −0.003 Hz. Based on the plotted extrema, the adaptive controller reduces the peak visible frequency deviation by approximately 40%. The improvement is most apparent around the major load/PV transitions near 6 s, 8 s, 10 s, and 12 s.

The RoCoF response provides stronger separation between the two controllers. The largest visible droop excursion is approximately +0.42–0.43 Hz/s, with a negative excursion of about −0.33 Hz/s. The adaptive VSG is visibly lower, with peaks of approximately +0.14 Hz/s and −0.22 Hz/s. The adaptive controller therefore substantially suppresses the fastest frequency transients in the displayed test.

The voltage response reveals the principal trade-off in the current tuning. Conventional droop remains approximately between 396 and 403 V, or about −1.0% to +0.75% relative to 400 V. Adaptive VSG reaches approximately 384–416 V, corresponding to roughly −4.0% to +4.0%. Although the adaptive VSG improves frequency and RoCoF, its present voltage loop therefore requires retuning.

The battery-power trace confirms active compensation of renewable/load imbalance, with positive power denoting discharge. The adaptive VSG reaches approximately +23 kW during the major deficit interval, while the droop response peaks near +20 kW. Both controllers reach close to −40 kW during

charging intervals, indicating that the battery is used aggressively to absorb both renewable deficits and surplus-generation events.

The SOC changes only from approximately 80.00% to 80.07% over the 15-s simulation. The nearly flat SOC is physically consistent with the short simulation duration relative to a 100-kWh battery, but it cannot demonstrate long-duration energy resilience; longer-duration tests are required.

The DC-link voltage exhibits large excursions and repeatedly reaches the imposed model bounds of approximately 550 V and 800 V. The 700-V reference is therefore not maintained throughout the disturbance sequence. This is a significant limitation because DC-link saturation can mask the AC-side controller's true performance. Resilience therefore requires simultaneous monitoring of AC frequency, AC voltage, and DC-link voltage.

The power factor is close to unity during most high-load periods, but the adaptive VSG falls to approximately 0.78 during the final low-load interval, whereas the droop trace remains near 0.95. The efficiency indicator also shows abrupt changes and low values at low power. These results indicate that low-load operation needs separate evaluation, and that efficiency and PF are useful monitoring variables but should not be used as primary evidence of resilience until the converter loss model and reactive-power control are refined.

4.1 Current and harmonic indicator

The AC current reaches approximately 68–70 A during the 45-kW high-load periods, consistent with 45 kW active power plus approximately 15 kvar reactive power at 400 V three-phase. The modeled voltage THD remains almost exactly 3.354% throughout the simulation for both controllers. Because the THD trace is constant in both cases, it is an analytical/modeled indicator rather than a waveform-derived FFT measurement; it demonstrates only that the model assigns the same THD indicator to both controllers and does not establish harmonic performance compliance. Future validation should use switching-level waveforms and FFT-based THD calculations.

Table 2. Approximate performance values extracted from the simulation plots.

Performance variable	Conventional droop	Adaptive VSG
Peak visible |Δf|	≈ 0.0048 Hz	≈ 0.003 Hz
Peak visible RoCoF	≈ +0.42 / −0.33 Hz/s	≈ +0.14 / −0.22 Hz/s
AC RMS voltage range	≈ 396–403 V	≈ 384–416 V
Peak battery discharge	≈ +20 kW	≈ +23 kW
Peak battery charge	≈ −40 kW	≈ −40 kW
SOC range	≈ 80.00–80.07%	≈ 80.00–80.07%
DC-link voltage	≈ 550–800 V	≈ 550–800 V
Final low-load PF	≈ 0.95	≈ 0.78
AC current at 45-kW load	≈ 68–70 A	≈ 65–69 A
Modeled voltage THD	≈ 3.354%	≈ 3.354%

5 Resilience performance indices

The indices proposed for assessing resilience in future validation are listed in Table 3.

Table 3. Resilience performance indices.

Index	Expression	Purpose
Frequency deviation	$\max\|f - f_0\|$	Frequency stability
RoCoF	$\max\|\mathrm{d}f/\mathrm{d}t\|$	Fast frequency response
Voltage deviation	$\max\|V - V_0\|$	Voltage stability
DC-link deviation	$\max\|V_{dc} - V_{dc,0}\|$	Converter energy balance
Battery stress	$\max\|P_B\|, \int P_B^2\,\mathrm{d}t$	Storage stress
SOC reserve	min SOC	Energy security
IAE	$\int\|e\|\,\mathrm{d}t$	Overall transient error
ISE	$\int e^2\,\mathrm{d}t$	Penalty on large excursions
THD	FFT spectrum	Harmonic impact
Recovery time	Time to tolerance band	Resilience/recovery

6 Discussion of baseline controller trade-offs

The baseline results yield a key finding: adaptive VSG performance should not be evaluated solely on frequency. The current tuning improves frequency and RoCoF, but it is less favorable for AC voltage and requires significant battery intervention. Therefore, the appropriate research objective is multi-objective resilience rather than single-variable frequency optimization. A suitable composite objective function is

$$J = w_f \mathrm{IAE}_f + w_v \mathrm{IAE}_V + w_r \mathrm{IAE}_{RoCoF} + w_b J_{BESS} + w_{dc} \mathrm{IAE}_{V_{dc}} + w_h \mathrm{THD} \tag{6}$$

The weights should be selected based on engineering requirements rather than chosen solely to make one controller appear better. The optimization should also include hard constraints on frequency, voltage, DC-link voltage, battery current, SOC, and converter apparent power.

7 Novelty and research contribution

A distinguishing feature of this work is the resilient adaptive grid-forming control structure, wherein disturbance severity modulates virtual inertia, damping, voltage-control gains, and battery support. This approach establishes a direct relationship between measurable microgrid operating conditions and control actions.

The proposed resilient adaptive grid-forming control framework translates renewable/load disturbance severity and battery state into coordinated virtual-inertia, damping, voltage-support, and battery-energy-management actions for a renewable-rich islanded microgrid.

This positioning is supported by the VSG and microgrid-control literature, which establishes the role of virtual inertia, damping, and coordinated control in converter-dominated islanded systems [1]–[6], while recent adaptive-VSG studies demonstrate the value of disturbance-dependent parameters for frequency stability [7]–[9].

8 Limitations

The three supplied simulation figures provide the principal baseline dynamic results for this paper. They compare conventional droop and adaptive VSG under the same 15-s load/PV disturbance sequence. The model is also averaged; the THD quantity is a modeled indicator rather than an FFT measurement, and the DC-link signal repeatedly reaches imposed hard bounds.

The appropriate claim is that a baseline adaptive-VSG response has been established under load and PV disturbances, and that a resilience framework has been defined for future validation against additional disturbance classes.

9 Conclusion

This paper developed a resilient adaptive VSG framework using the supplied 50-kW PV–battery islanded-microgrid simulations as the baseline. The results show that adaptive VSG reduces the visible frequency and RoCoF excursions compared with conventional droop under the tested load/PV disturbances. However, the same tuning produces substantially larger AC-voltage excursions and a more aggressive battery response, demonstrating that frequency improvement alone is insufficient to establish overall resilience.

The principal conclusion is therefore that resilience must be formulated as a coordinated frequency–voltage–DC-link–battery problem. Future work should replace the current hard DC-link bounds with physically parameterized converter dynamics, refine the adaptive voltage loop, add explicit secondary control, validate harmonic distortion using waveform FFT, and test the framework under longer-duration and external-disturbance scenarios.

References

[1] Zhong QC, Weiss G. Synchronverters: inverters that mimic synchronous generators. *IEEE Trans. Ind. Electron*. 2011;58(4):1259–1267. https://doi.org/10.1109/TIE.2010.2048839

[2] Guerrero JM, Vasquez JC, Matas J, de Vicuña LG, Castilla M. Hierarchical control of droop-controlled AC and DC microgrids—a general approach toward standardization. *IEEE Trans. Ind. Electron*. 2011;58(1):158–172. https://doi.org/10.1109/TIE.2010.2066534

[3] Rocabert J, Luna A, Blaabjerg F, Rodriguez P. Control of power converters in AC microgrids. *IEEE Trans. Power Electron*. 2012;27(11):4734–4749.

[4] Beck HP, Hesse R. Virtual synchronous machine. In: *Proc*. 9th Int. Conf. Electrical Power Quality and Utilization. Barcelona, Spain; 2007.

[5] Awal MA, Yu H, Tu H, Lukic S, Husain I. Review on virtual synchronous generator model and control for improving microgrid stability. In: *Proc*. 7th Int. Conf. Electrical Energy Systems. 2021. https://doi.org/10.1109/ICEES51510.2021.9383646

[6] Bevrani H, Ise T, Miura Y. Virtual synchronous generators: a survey and new perspectives. *Int. J. Electr. Power Energy Syst*. 2014;54:244–254. https://doi.org/10.1016/j.ijepes.2013.07.009

[7] Fathi A, Shafiee Q, Bevrani H. Robust frequency control of microgrids using an extended virtual synchronous generator. *IEEE Trans. Power Syst*. 2018;33(6):6289–6297. https://doi.org/10.1109/TPWRS.2018.2850880

[8] Pournazarian B, Sangrody R, Lehtonen M, Gharehpetian GB, Pouresmaeil E. Simultaneous optimization of virtual synchronous generators parameters and virtual impedances in islanded microgrids. *IEEE Trans. Smart Grid*. 2022;13(6):4202–4217. https://doi.org/10.1109/TSG.2022.3186165

[9] Pouresmaeil M, Sangrody R, Taheri S, Pouresmaeil E. An adaptive parameter-based control technique of virtual synchronous generator for smooth transient between islanded and grid-connected mode of operation. *IEEE Access*. 2021;9:137322–137337. https://doi.org/10.1109/ACCESS.2021.3117617

[10] IEEE standard for the specification of microgrid controllers. *IEEE Std 2030.7-2017*. IEEE; 2018.

[11] IEEE standard for the testing of microgrid controllers. *IEEE Std 2030.8-2018*. IEEE; 2018.

[12] IEEE recommended practice for the planning and design of the microgrid. *IEEE Std 2030.9-2019*. IEEE; 2019.

[13] IEEE standard for interconnection and interoperability of distributed energy resources with associated electric power systems interfaces. IEEE Std 1547-2018 (amended by IEEE Std 1547a-2020). IEEE; 2018.

[14] IEEE standard for harmonic control in electric power systems. *IEEE Std 519-2022*. IEEE; 2022.

[15] Communication networks and systems for power utility automation—Part 7-420: Basic communication structure—Distributed energy resources and distribution automation logical nodes. IEC 61850-7-420:2021, 2nd ed. International Electrotechnical Commission; 2021.